Ultrafast microfluidics using surface acoustic waves

Leslie Y. Yeo[a] and James R. Friend
Micro/Nanophysics Research Laboratory, Monash University, Clayton, VIC 3800, Australia

(Received 21 November 2008; accepted 2 December 2008; published online 2 January 2009)

We demonstrate that surface acoustic waves (SAWs), nanometer amplitude Rayleigh waves driven at megahertz order frequencies propagating on the surface of a piezoelectric substrate, offer a powerful method for driving a host of extremely fast microfluidic actuation and micro/bioparticle manipulation schemes. We show that sessile drops can be translated rapidly on planar substrates or fluid can be pumped through microchannels at 1–10 cm/s velocities, which are typically one to two orders quicker than that afforded by current microfluidic technologies. Through symmetry-breaking, azimuthal recirculation can be induced within the drop to drive strong inertial microcentrifugation for micromixing and particle concentration or separation. Similar micromixing strategies can be induced in the same microchannel in which fluid is pumped with the SAW by merely changing the SAW frequency to rapidly switch the uniform through-flow into a chaotic oscillatory flow by exploiting superpositioning of the irradiated sound waves from the sidewalls of the microchannel. If the flow is sufficiently quiescent, the nodes of the transverse standing wave that arises across the microchannel also allow for particle aggregation, and hence, sorting on nodal lines. In addition, the SAW also facilitates other microfluidic capabilities. For example, capillary waves excited at the free surface of a sessile drop by the SAW underneath it can be exploited for micro/nanoparticle collection and sorting at nodal points or lines at low powers. At higher powers, the large accelerations off the substrate surface as the SAW propagates across drives rapid destabilization of the drop free surface giving rise to inertial liquid jets that persist over 1–2 cm in length or atomization of the entire drop to produce 1–10 μm monodispersed aerosol droplets, which can be exploited for ink-jet printing, mass spectrometry interfacing, or pulmonary drug delivery. The atomization of polymer/protein solutions can also be used for the rapid synthesis of 150–200 nm polymer/protein particles or biodegradable polymeric shells in which proteins, peptides, and other therapeutic molecules are encapsulated within for controlled release drug delivery. The atomization of thin films behind a translating drop containing polymer solutions also gives rise to long-range spatial ordering of regular polymer spots whose size and spacing are dependent on the SAW frequency, thus offering a simple and powerful method for polymer patterning without requiring surface treatment or physical/chemical templating.
[DOI: 10.1063/1.3056040]

I. INTRODUCTION

Since the inception of the "lab-on-a-chip" concept, considerable effort has been made to develop strategies for reliable and efficient microfluidic actuation and manipulation. The challenge, is, of course, to overcome the large surface and viscous forces that resist fluid motion at very small scales, wherein inertia and other driving forces tend to be negligible in most microflu-

[a]Electronic mail: leslie.yeo@eng.monash.edu.au.

idic systems—we mention most here because, as we shall discuss subsequently, it is indeed possible that inertia can arise in microfluidic flows. A variety of overarching mechanisms have been proposed for driving microscale fluid motion as well as particle or biomolecule manipulation. These can be generally classified by the nature of the external force employed to drive the fluid motion:[1] pressure gradient, capillary, electric, magnetic, and acoustic.

Curiously, acoustically driven microfluidic actuation mechanisms, often considered a subset of acoustofluidics wherein the application of an acoustic force on a fluid gives rise to an acoustic radiation force as well as acoustic streaming (time-averaged bulk viscous fluid motion), have, to date, received little attention compared to the other mechanisms, in particular, electrokinetically driven mechanisms. This is somewhat surprising given that, as one prominent review article on microfluidics puts it, "acoustic streaming represents one of the very few inertial phenomena that may actually play a significant role in microfluidic devices."[2] In contrast, the Reynolds number Re associated with other microfluidic actuation mechanisms is considerably lower, in the range $\mathrm{Re} \lesssim 1$ wherein viscous dominance render fluid inertia and its associated nonlinearities irrelevant. Such low Reynolds number hydrodynamics essentially pose significant challenges in microfluidics, not least the low actuation speeds for micropumping and the difficulty in generating turbulent vortices for micromixing.

Admittedly, conventional acoustically driven microfluidic mechanisms, particularly that driven by ultrasonic bulk waves at lower kilohertz (kHz) order frequencies, suffer from certain limitations that render them less attractive when compared alongside electrokinetic devices. Primarily, at the low frequencies associated with typical ultrasonic mechanisms, the millimeter order wavelengths are typically incompatible with microfluidic devices, which have characteristic length scales that are at least one order of magnitude smaller, and with biomolecules which have sizes that are several orders smaller. In addition, there is a common perception that the bulk motion of mechanical parts such as vibrating flexural plates at these scales are less reliable and more prone to wear and tear. Cost is also a factor, and often acoustic microdevices are severely restricted owing to the choice of piezoelectric materials. It is also questionable whether the fluid-structural interactions are adequately energy efficient to render acoustically driven mechanisms sufficiently attractive relative to other actuation mechanisms. Furthermore, most traditional forms of acoustic excitation employ bulk waves that require careful design in mounting and application to prevent their loss or conversion, especially at the small scales pertinent to microfluidic applications. Moreover, at low (kHz order) frequencies, cells are susceptible to denaturing due to the large shear forces induced along the cellular membrane. In fact, sonoporation,[3] which employs acoustically induced microbubble pulsation, is a common technique for cell membrane poration as a procedural step for biomolecular transfection and intracellular loading. This risk of cell lysis also renders cavitation streaming unsuitable for biological microfluidics.

A less conventional method for acoustic driving of microfluidic flows, however, has demonstrated exceptional promise. Surface acoustic wave (SAW) microfluidic actuation retains the benefits of using acoustic fields for driving fluid motion, namely, the large actuation speeds and the associated flow nonlinearities rendered by the inertial forcing, while addressing the limitations discussed above that plague conventional ultrasonic methods. Surface acoustic waves are nanometer order amplitude electroelastic waves that propagate along the surface of a piezoelectric substrate. Most importantly, the megahertz (MHz) order SAW vibrations facilitate fluid and particle manipulation at a much finer scale that is commensurate with microfluidic devices; in Sec. II B, we shall also show that the high frequencies employed have time scales that are too short to generate shear gradients that could cause cell membrane lysis or trigger apoptotic pathways. As shown in Fig. 1(a), the SAW, here in the form of a Rayleigh wave[4] in which the axial displacement of the solid elements are polarized normally to the surface, is isolated within 4–5 wavelengths (typically, $\lambda \sim 100\ \mu\mathrm{m}$) of the substrate surface—the dispersion associated with the localization of energy along a very narrow surface region is thus far less than bulk waves; less power is therefore necessary to drive fluid flow due to the ability to concentrate the energy into the fluid without requiring the use of acoustic focusing lenses, rendering the mechanism more energy efficient than prior approaches. This is particularly important in microfluidic devices where true miniaturization

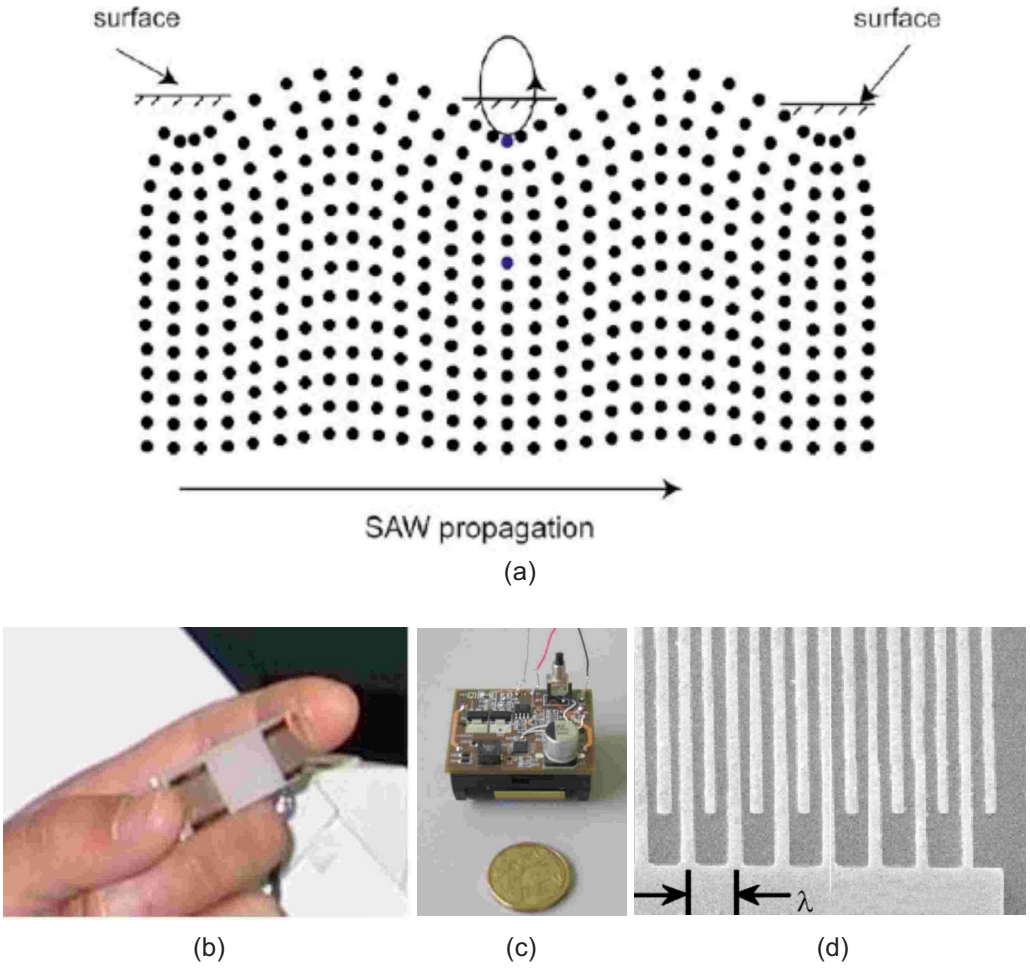

FIG. 1. (a) Schematic depiction of a SAW propagating on the surface of a piezoelectric substrate. Note the localization of the Rayleigh wave on the surface, which decays exponentially into the substrate such that the motion is negligible at a depth of 4–5 SAW wavelengths into the substrate. (b) Image of the SAW device consisting of the piezoelectric substrate on which the SAW propagates, (c) the portable power supply used to generate the SAW, and, (d) the interdigitated transducers (IDTs) patterned onto the piezoelectric substrate.

involves not just scale down of the fluid housing (e.g., microchannels) and components (e.g., micropumps, microreactors, microseparators, etc.), but also the characterization and detection methods (e.g., sensing devices) and power supplies. Figures 1(b) and 1(c) show the typical size of the SAW substrate and power supply used to drive microfluidics in our laboratory, thus demonstrating a fully portable scale device.

In fact, SAWs have been commonly used for decades, although not for microfluidic actuation. Soon after a convenient method for generating them was discovered,[5] SAWs have since been employed in the telecommunications industry for signal processing and bandpass filtering; there is, on average, four SAW devices in every mobile phone.[6] Other applications for SAWs are found in automotive windscreen raindrop sensors, touch sensitive screens, and chemical/biological sensors. The wide range of SAW applications show, at least, the commercial viability of these devices. With advances in nanofabrication technology, SAW devices can be mass produced at relatively low cost. Moreover, the development of SAW devices in these applications has advanced to a state where these devices are extremely reliable.

The SAW devices employed in our discussion here consist of a double port interdigitated transducer (IDT) with a number (around 25) of 400 nm thick, straight aluminum electrode pairs

sputter-deposited onto a single crystal 127.68° *yx*-cut lithium niobate ($LiNbO_3$) piezoelectric crystal substrate, as shown in Figs. 1(b) and 1(d). The IDTs are fabricated using standard ultraviolet photolithography and wet etch techniques. To generate the SAW, an oscillating electrical signal matching the operating frequency is applied to the IDT using a radio frequency (rf) signal generator and power amplifier. The SAW, which propagates across the substrate as a Rayleigh wave, then has wavelength λ which is set by the IDT finger width and spacing, both of which are $\lambda/4$. This determines the SAW resonant frequency (and hence, the operating frequency) $f=c_s/\lambda$, where $c_s \approx 3965$ m/s is the speed of the SAW in the substrate. In place of a traveling SAW, a standing SAW can also be generated by incorporating a reflector IDT at the opposite end, as shown in Fig. 1(b).

II. SAW-DRIVEN MICROFLUIDICS

The ability for the SAW to drive microfluidics arises due to the fluid-structural coupling. To illustrate this, consider a liquid drop placed on the substrate in between the IDTs such that it is within the propagation pathway of the SAW, as depicted in Fig. 2(a). When the SAW comes into contact with the edge of the drop, the acoustic energy diffracts into the drop due to the mismatch between the sound velocity in the substrate c_s and that in the liquid, c_l ($\approx$1485 m/s for water), as shown in Fig. 2(b). In fact, the angle at which the SAW diffracts into the drop is specified by the ratio between the sound velocities, and is referred to as the Rayleigh angle $\theta_R=\sin^{-1}(c_l/c_s) \approx 22°$ [Fig. 2(b)]. Known as leaky SAW, this energy transfer into the drop gives rise to a longitudinal pressure wave front that drives bulk liquid recirculation within the drop, or acoustic streaming. In addition, the horizontal component of the energy transfer into the drop at the Rayleigh angle gives rise to a body force on the entire drop in the direction of propagation of the SAW. This can be seen by the deformation of the drop into an asymmetrical conical structure, which leans over at the Rayleigh angle, as shown in Fig. 2(c).

Figure 3 shows the different responses of the liquid drop to the substrate vibration in the order of increasing rf power applied to the IDTs. At low powers, the drop deforms into the axisymmetrical conical shape and leans at the Rayleigh angle, as discussed previously. Nevertheless, even at these low powers, the capillary vibration at the drop's free surface has implications for particle assembly and sorting as will be discussed subsequently in Sec. II A. As the power is increased, sufficient body forces on the drop then build up and cause the drop to translate—such motion can be exploited for moving and manipulating drops in open microfluidic circuits, as will be discussed in Sec. II B. If the drop was constrained, for example, by patterning a circular section of a hydrophobic substance, e.g., Teflon AF®, onto the substrate, the concentration of energy along the substrate at the base of the drop, and subsequently its leakage into the drop, will result in a peculiar jetting phenomenon (Sec. II E), or, at the high end of the power spectrum, atomization of the entire drop (Sec. II F).

In what follows, we will discuss each of these microfluidic schemes, as well as other derivatives, and their potential for application in practical microfluidic systems. The overarching theme of these different manipulations is the simplicity of the device for generating the desired inertia-dominant fluid/particle motion as well as the sheer speeds by which these can be carried out in comparison with the most advanced microfluidic capabilities available at present.

A. Drop vibration and particle assembly

If the drop was to comprise of a colloidal suspension of nanoparticles, the low power vibration of the drop induced by the SAW causes a unique particle assembly phenomenon.[7] Figure 4 shows a delineation of the interesting particle assembly patterns that arise on the free surface of the drop with a given diameter. Initially, the colloidal particles assemble into linear concentric rings as shown by the fingerprint-like patterns in regime A. Curiously, the separation between the rings is roughly 100 μm, corresponding to half the SAW wavelength, i.e., $\lambda/2$. A frequency scan using laser Doppler vibrometry (LDV) indicates that the drop's free surface is vibrating at the same frequency (20 MHz) as the SAW vibration induced on the surface of the substrate beneath it,

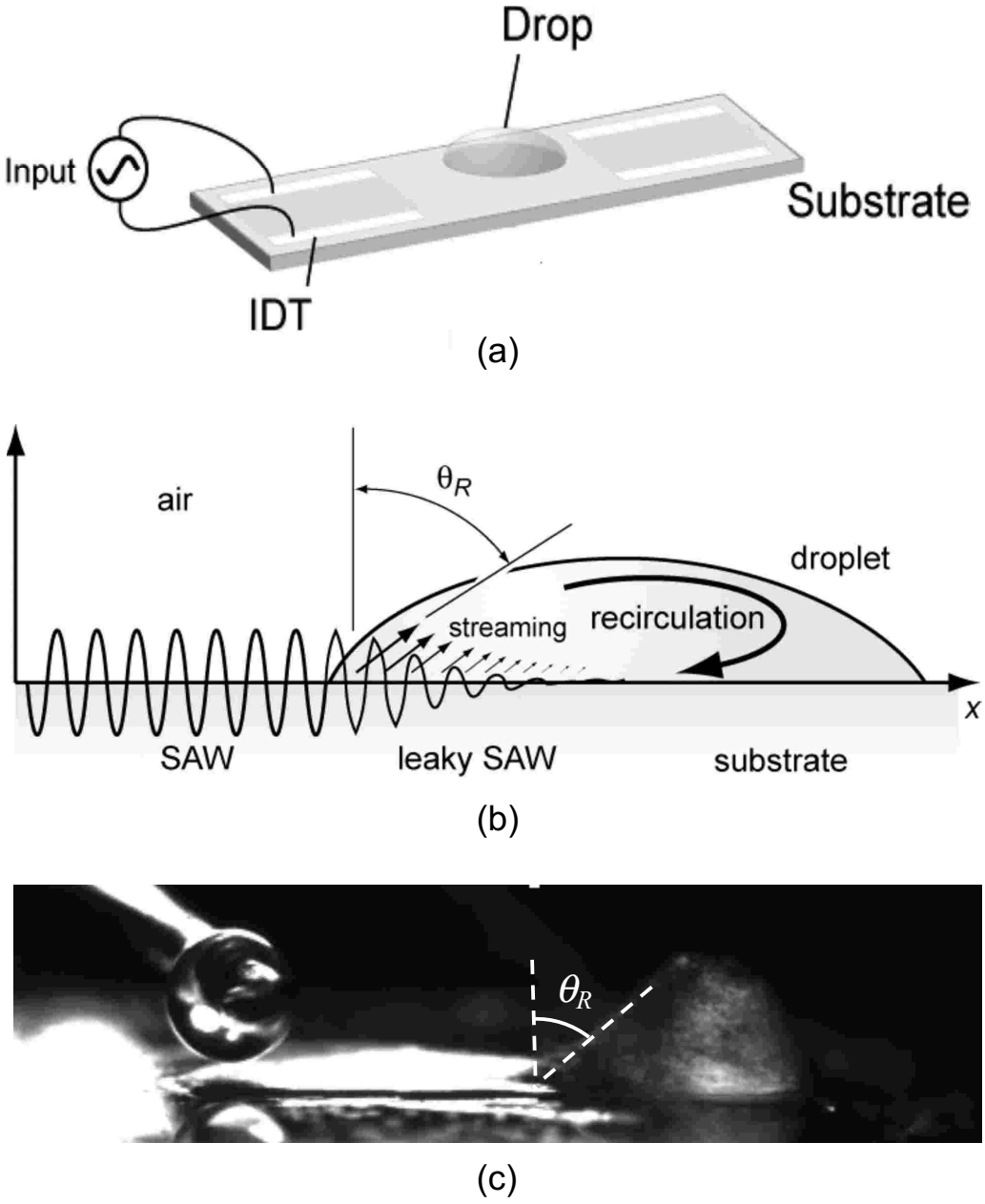

FIG. 2. (a) Schematic depiction of a liquid drop placed on the substrate in the propagation pathway of the SAW. (b) Due to the different sound velocities in the substrate and in the liquid phases, the SAW energy leaks into the drop at a specific angle, the Rayleigh angle θ_R, as it comes into contact with the drop. This gives rise to bulk liquid recirculation (acoustic streaming) within the drop and a body force on the drop itself in the SAW propagation direction. (c) The body force on the drop causes the drop to deform into an axisymmetrical conical shape whose trailing edge leans at the Rayleigh angle and subsequently to translate across the substrate.

albeit at lower amplitudes. It is thus conceivable that the linear colloidal ringlike assemblies coincide with the nodal lines of these low amplitude 20 MHz standing wave vibrations induced along the drop interface. A possible mechanism by which the particles drift to form these patterns is due to the capillary force acting on the particles in concert with the surface acceleration of the standing wave vibration, first proposed by Falkovich *et al.*[8] to elucidate the well-known observation that hydrophillic particles assemble onto the nodal lines of a standing wave induced along a liquid free surface whereas hydrophobic particles assemble onto the antinodal lines. The inverse of

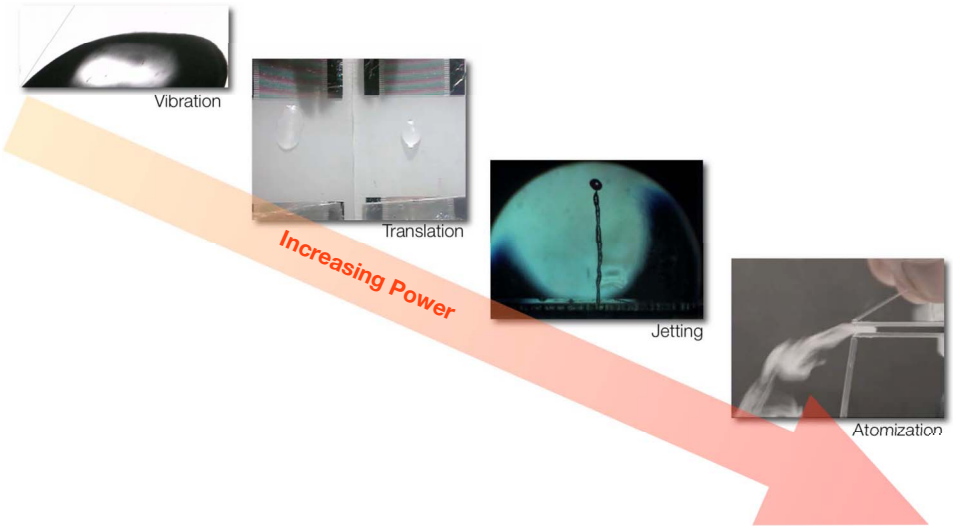

FIG. 3. Typical microfluidic manipulations that arise due to the fluid-structural interaction between the SAW and a liquid drop placed on the SAW substrate. In the order of increasing rf power applied to the IDTs, the drop vibrates, translates (the left image shows the translation of a drop on the bare lithium niobate substrate, which is hydrophilic, and the right image shows the same drop translating on a substrate which has been coated with a hydrophobic substance), forms a long slender jet, and, eventually atomizes.

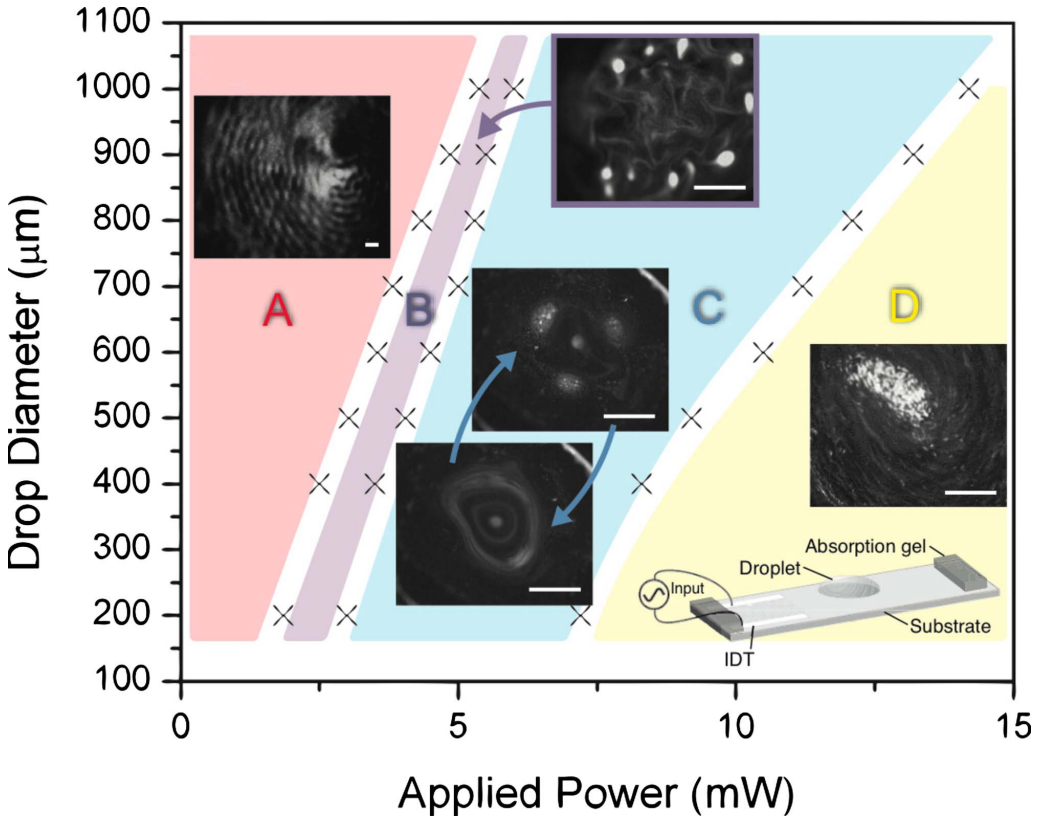

FIG. 4. Interfacial colloidal patterns as a function of the initial drop diameter and input power induced by low power SAW drop vibration (Ref. 7). The scale bars in the image indicate a length scale of 200 μm.

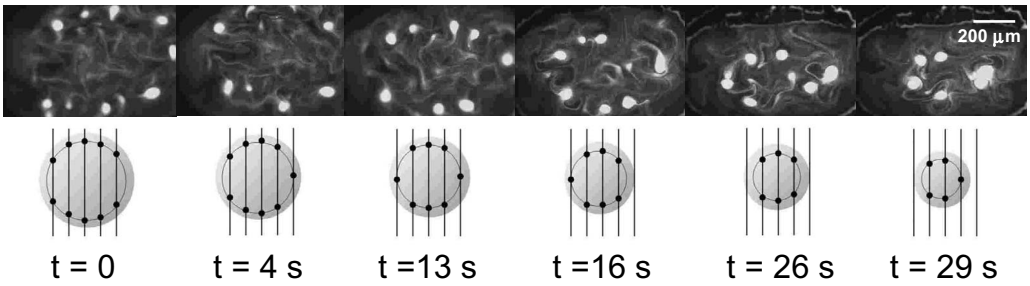

FIG. 5. The number of colloidal islands formed depends on the drop size which decreases due to evaporation in time. The bottom schematic shows the successive decrease in the number of intersection points between the 20 MHz nodal lines and the 1 kHz circular nodal ring as the drop and hence the nodal ring shrinks (Ref. 7).

the time taken for the particles to assemble into the ringlike assemblies is observed to scale linearly with the square of the vibration amplitude, consistent with that observed in Falkovich *et al.*,[8] thus inspiring confidence that the particle drifting mechanism is indeed a plausible mechanism to explain how the particles assemble onto the nodal lines.

Upon increasing the input power, and hence, traversing into regime B, the colloidal particles in the linear ringlike assemblies are observed to cluster to form pointwise colloidal islands, as illustrated in Fig. 4. We note that this regime is associated with an increase in the magnitude of the interfacial vibration. A repeat of the LDV frequency sweeps revealed that, in addition to the small amplitude 20 MHz standing wave vibrations at the drop interface, large amplitude 1 kHz order vibrations were also significant in this regime; these large amplitude low frequency vibrations are associated with the capillary-viscous resonance of the drop. The colloidal islands therefore appear to form at the intersection between the nodal lines of the low amplitude 20 MHz standing wave vibration and the circular nodal ring of the large amplitude 1 kHz vibration associated with the capillary-viscous resonance of the drop. As in regime A, the inverse of the time it takes for the particles to cluster into these pointwise assemblies again scales with the square of the amplitude of the vibration, therefore suggesting the same particle drift mechanism as before.

The number and position of the colloidal island assemblies depends on the size of the drop. If the input power is kept constant and the drop is allowed to evaporate, the number of islands decreases successively, as seen in Fig. 5. This peculiar phenomenon can be explained with reference to the Rayleigh–Lamb dispersion relationship. As the drop evaporates and hence its size decreases, the capillary-viscous resonant frequency at which the drop vibrates increases, resulting in a decrease in the corresponding wavelength. Consequently, the size of the circular nodal ring shrinks. If the wavelength of the low amplitude 20 MHz interfacial vibration, and hence, the separation between the linear nodal lines is assumed constant, then an intersection point (and hence, a colloidal island) is sequentially lost as the nodal ring decreases in size.

Further increases in the input power into regime C leads to the onset of significant fluid streaming within the drop. Such azimuthal fluid recirculation in the drop will be further discussed in Sec. II D. Briefly, however, when streaming commences, the particles are dispersed, and hence, the colloidal island assemblies are destroyed (Fig. 4). However, after a short transient, the streaming ceases and the colloidal islands are observed to reform until the streaming recommences and erases them again, as depicted in Fig. 6. This cyclic phenomenon occurs aperiodically and the direction of the streaming (clockwise/anticlockwise) is noted to be reasonably random, suggesting that this regime is a transient metastable state and that the commencement and cessation of the streaming is triggered by a peculiar instability arising from the highly nonlinear coupling between the acoustic, hydrodynamic and capillary forces. As the input power is increased (regime D), however, the streaming becomes stronger and more consistent, leading to permanent dispersion of the particles (Fig. 4), as will be discussed in Sec. II D. Once this occurs, the interfacial colloidal patterns are no longer evident.

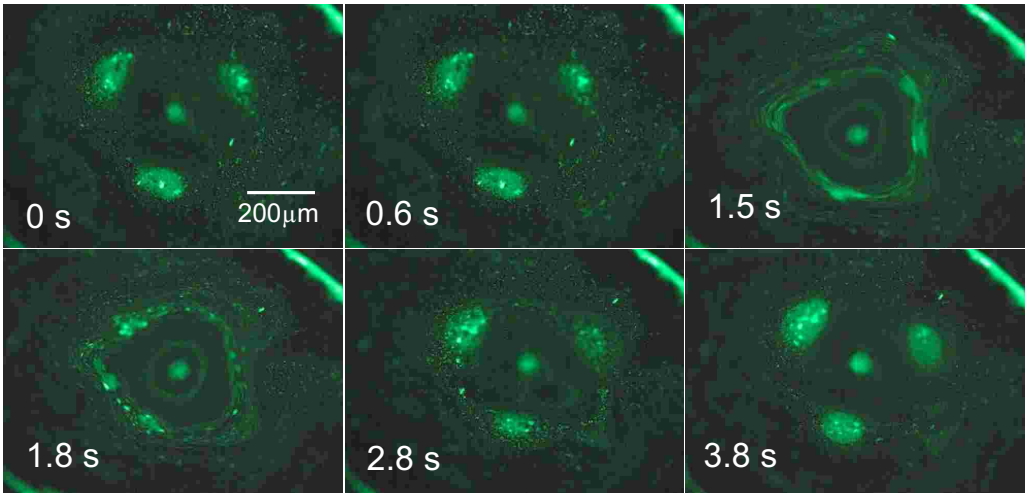

FIG. 6. Metastable transient state in which the system cycles randomly between colloidal island formation when there is no streaming and colloidal island erasure when streaming commences (Ref. 7).

B. Drop translation and particle collection

As described in Sec. II, drops can be translated on the SAW substrate due to the body force generated on the drop as a consequence of the radiation leakage into the drop at the Rayleigh angle. The drop translation speeds are extremely fast, around 1–10 cm/s (Refs. 9 and 10), and one to two magnitudes larger than the speeds that can be achieved through other microfluidic actuation mechanisms, for example, electrowetting.[11] Such ability to move drops on planar substrates is especially useful in open microfluidic systems in which discrete drops are transported and manipulated as opposed to closed microfluidic systems in which the liquid is housed in microchannels. Although not particularly suited for continuous flow analysis and particularly when larger liquid volumes are involved, open systems offer the possibility of scaleability and reconfiguration such that analyses can be carried out in similar fashion to traditional benchtop protocols.[12] Besides, drops are often useful as carriers for biological entities, and hence, different biological agents can be transported separately in different drops without coming into contact with the other. Another advantage of open microfluidic systems is the ability to minimize the amount of liquid required as well as the contact between the liquid and solid surface, especially crucial in applications that involve biomolecules in which surface adsorption is undesirable. Protein adsorption is commonly due to electrostatic interactions and the degree to which it occurs is dependent on the charge, polarity on the protein as well as the applied voltage.[13] The open system also eliminates the attenuation of detection signals through channel walls although it is prone to contamination and evaporation. A possible way to circumvent this problem is to confine the system within an oil medium, which has also been found to suppress adsorption.[14]

Indeed, SAW-driven drop translation has been employed for various biological applications. Tan *et al.*[10] demonstrated that this mechanism allows for rapid and efficient uptake of microparticles on a substrate, for example, in biosensors for environmental air monitoring, which requires the collection and concentration of airborne particulates into a carrier for subsequent detection (Fig. 7). As the drop translates across a surface dusted with these microparticles, the acoustic streaming within the drop aids in sweeping up the particles from underneath the drop into its bulk.

Another application for the SAW-driven drop translation is in the fast and effective seeding of cells into porous bioscaffolds for tissue/bone regeneration.[15] Static seeding methods, which rely on gravity-driven perfusion, are extremely slow (typically hours to weeks) given the large capillary resistances imposed by the small 100 μm order pore sizes whereas bulk seeding methods which employ bioreactors that work on the principle of agitation, vacuum suction, or sedimentation, for example, lack the ability for fine control that microfluidic systems offer. By rapidly moving a drop

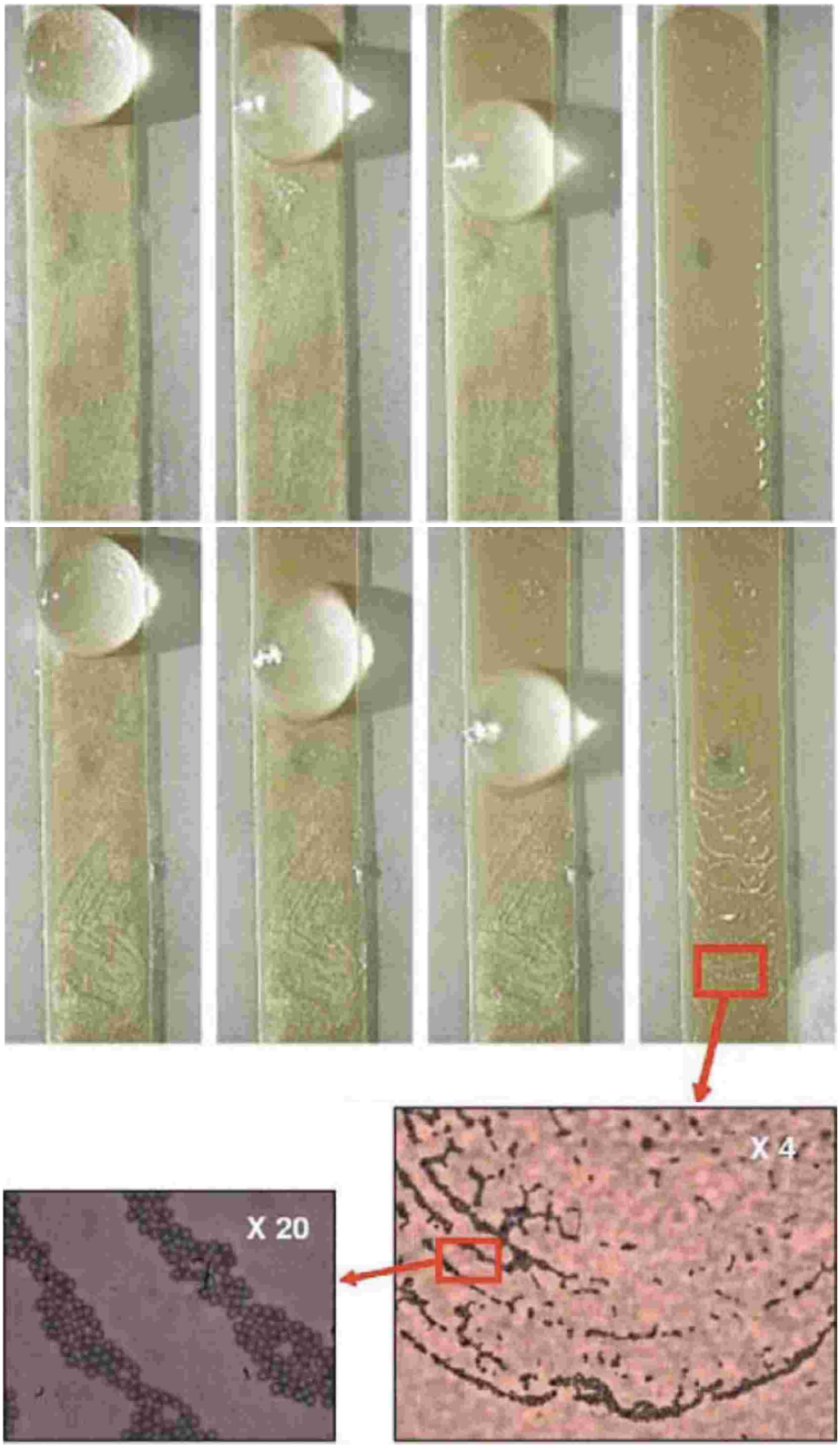

FIG. 7. Rapid and efficient collection and concentration of microparticles on a substrate by sweeping carrier drops across the surface using the SAW (Ref. 10). The top image shows the collection of 10 μm melamine (hydrophilic) particles whereas the bottom image shows the collection of 10 μm polystyrene (hydrophobic) particles. The inset shows a magnification of the polystyrene particles left behind on the track, which assemble into concentric ring assemblies.

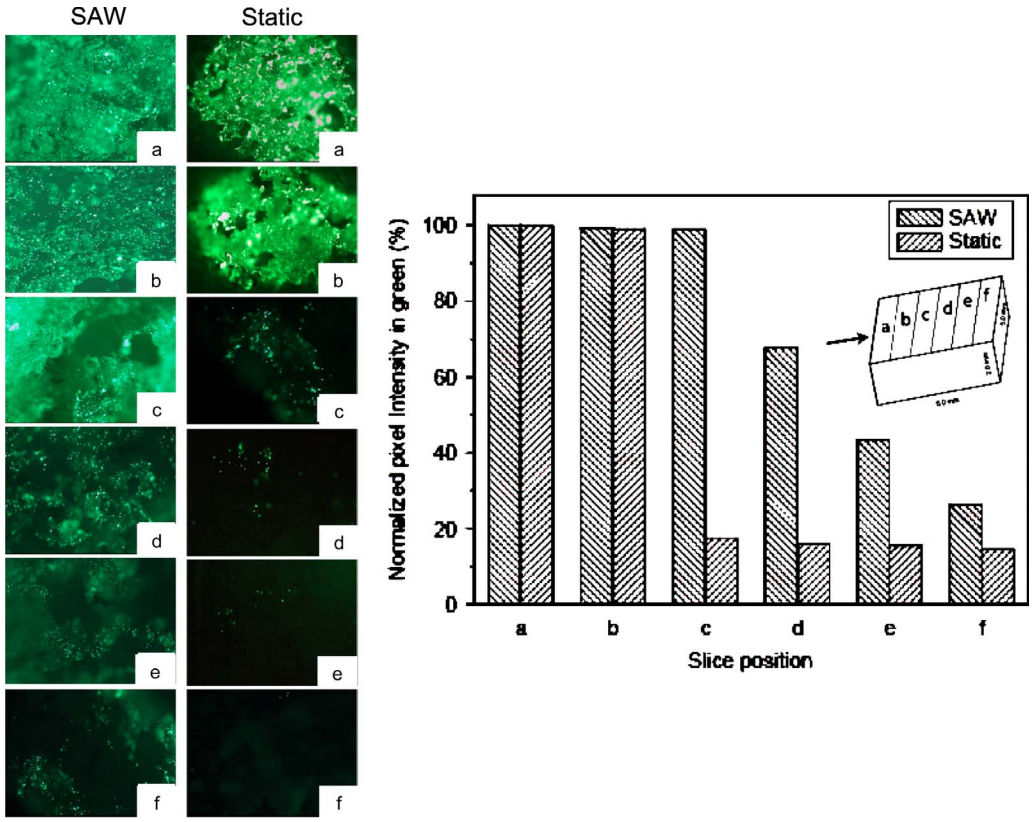

FIG. 8. Comparison between static (gravity perfusion) and SAW-driven cell seeding (Ref. 15). The images in the columns on the left show successive cross-sectional slices of the scaffold after the seeding, in this case using 5 μm fluorescent particles, has occurred. The slices a–f correspond to that in the schematic shown in the inset of the right image; the arrow shows the scaffold face along which the drop containing the cell suspension first enters. The first column in the left image shows the results of the SAW seeding whereas the second column in the left image shows that from the static seeding. The right image shows the normalized pixel intensity of the fluorescent particles in each scaffold slice for both seeding methods. Both sets of results indicate deeper and more uniform penetration with the SAW method.

containing a suspension of cells to be seeded towards a scaffold placed in its path, we have found that the seeding process can be significantly accelerated as well as improved. Cells are seeded into the scaffold in under 10 s. Moreover, SAW cell seeding also offers a greater penetration depth into the scaffold as well as more uniform seeding, in contrast to the static method which is often plagued by insufficient and superficial (cells seeded along scaffold periphery instead of deep within) penetration, as shown by the results in Fig. 8. Moreover, the rapid speed of the seeding with the SAW allows multiple drops to be sequentially driven into the scaffold. With every successive drop containing the cell suspension that is driven into the scaffold, we observe an additional 1 mm of seeding penetration.[16] The scanning electron microscopy (SEM) imaging of seeded yeast cells in Fig. 9(a) show that the cell size and morphology are preserved; no cell denaturing or fragmentation due to the SAW radiation is evident.[16] Preliminary tests using flow cytometry to sort the live and dead yeast as well as primary murine osteoblast cells together with absorbance spectra from standard colorimetric assays (MTT or fluorescence assays from the uptake of Alamar Blue, both indicators of chemical reduction in the growth medium, and hence, the proliferation ability of the post-SAW seeded cells) indicate little effect of the SAW irradiation on cell viability and growth [Figs. 9(b)–9(d)].[17]

Similar SAW-driven drop actuation mechanisms have also been used for open microfluidic systems for DNA amplification via polymerase chain reaction (PCR) and hybridization.[14] Drops carrying the PCR reagents are transported on a hydrophobically coated surface similar to that used in the particle collection/concentration and cell seeding applications described above, merged at an

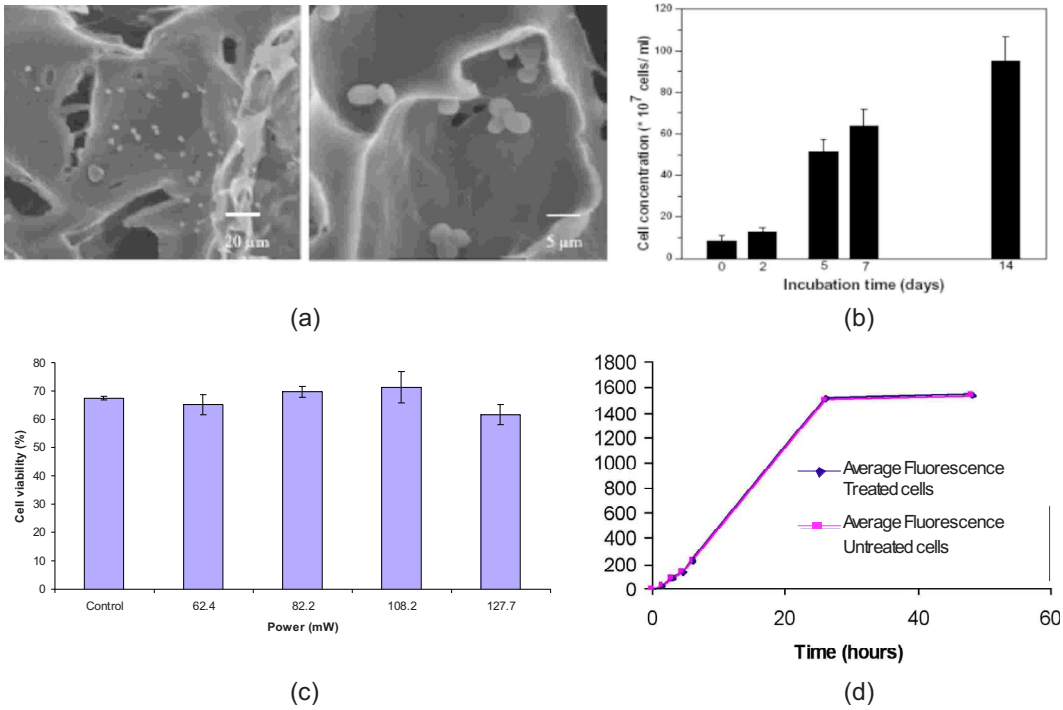

FIG. 9. (a) SEM images of yeast cells seeded into a poly(caprolactone) scaffold using SAW. The morphology of the cells do not appear to be compromised by the SAW radiation. (b) Proliferation rate of the yeast cells after irradiation with the SAW. Cells are observed to continue proliferating during the subsequent 14 days, which further confirms the viability of the yeast cells (Ref. 16). (c) Viability of primary murine osteoblast cells treated under the SAW irradiation at different rf powers. (d) Average cell proliferation of SAW-treated and untreated cells as function of the fluorescence intensity from the Alamar Blue uptake; the power of the SAW applied is 108.2 mW. In both (c) and (d), the cells were treated by the SAW at 20 MHz for 10 s, and the cell density and suspension volume is 5000 cells/μL and 10 μL, respectively.

intersection, and then subsequently moved to a position above an on-chip resistive heater to initiate the PCR reaction. For subsequent hybridization, the drop containing the PCR product is translated using the SAW to another position on the chip above a second heater where matched and mismatched oligonucleotides are spotted. Besides drop translation, the SAW can also be used to induce mixing to enhance the PCR reaction; we will discuss SAW-driven mixing strategies in subsequent sections.

C. Pumping and mixing in microchannels

Instead of free drop actuation in open microfluidic systems, the SAW can also be used to pump liquid through microchannels.[18–20] In Ref. 20, a poly(dimethylsiloxane) (PDMS) microchannel was mounted onto the SAW substrate, as shown in Fig. 10(a), whereas in Refs. 18 and 19, a microchannel was laser ablated into the substrate, as shown in Fig. 10(b). As with the SAW-driven drop transport, the micropumping velocities achieved are extremely high, on the order 1 cm/s, which is one to two decades larger than that possible with electrokinetic micropumps.[21]

Moreover, a peculiar attribute of the acoustic propagation in the fluid contained in the microchannel facilitates the ability to switch between uniform through-flow for fluid delivery and vortex-laden flows.[18,19] Figure 11(a) shows uniform fluid flow through a 50 μm microchannel. However, when the channel width W was increased while holding the input power and the SAW frequency constant, the flow becomes progressively irregular, as shown in Figs. 11(b)–11(d). More specifically, we observe uniform fluid flow when $W<\lambda_f$, where λ_f is the sound wavelength at the excitation frequency of the SAW in the fluid. As W increases beyond λ_f, vortices with characteristic length scales between 50 and 100 μm develop with an increasingly oscillatory flow structure.

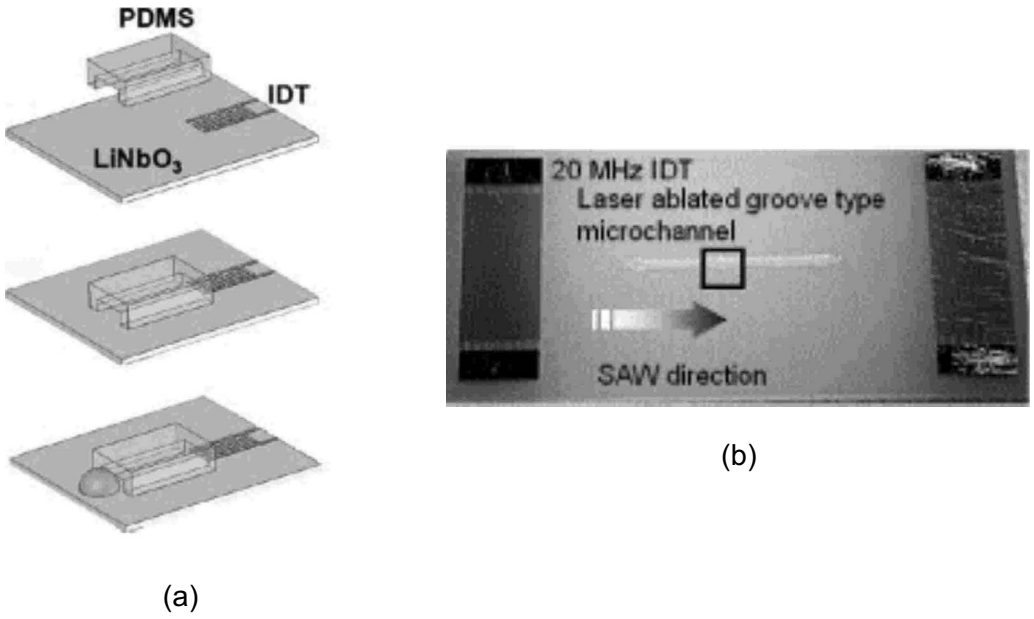

FIG. 10. SAW microchannel pumping configurations. (a) A PDMS microchannel is mounted on the SAW substrate (Ref. 20). (b) A microchannel is laser ablated into the SAW substrate (Refs. 18 and 19).

The vortices arise as a consequence of the sound waves irradiated from the sidewalls—since the transverse motions of the solid elements along the sidewalls are completely out-of-phase, the standing wave arising as a consequence of the superpositioning of the irradiated sound waves from the sidewalls of the microchannel can only occur if $W<\lambda_f$ and $W\neq n\lambda_f$, where $n=1,2,\ldots$. Given the transition from uniform through-flow in Fig. 11(a) to the oscillatory behavior exhibited in Figs. 11(b)–11(d) can be attributed to symmetry breaking of the instantaneous transverse velocity field, it then becomes clear why the transition is observed when $W>\lambda_f$.[18,19] In any case, the ability to rapidly switch between uniform through-flow and oscillatory vortical flows demonstrate the possibility for interchanging between pumping and mixing in the same microchannel simply by altering the SAW frequency, thus eliminating the elaborate architectures or separate components to induce mixing that are typically required in conventional microfluidic systems.[1]

Interestingly, if the fluid consisted of a suspension of colloidal particles, particle assembly also takes place in the regions where the fluid is quiescent, for example near the bottom of the microchannel. As shown in Fig. 12, linear particle arrangements assemble at the nodes of the pressure field corresponding with the first order fluid motion arising due to the compressibility of the sound waves that are radiated into the fluid. Note the correspondence between the number of nodal lines and the number of aligned particle assemblies. Specifically, the number of particle

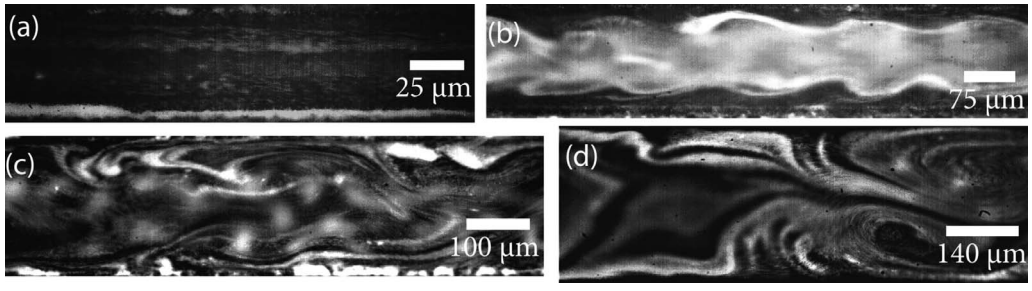

FIG. 11. Flow configuration as a function of channel width W. As $W>\lambda_f\approx 73$ μm, the uniform through-flow observed in image (a) is replaced by an oscillatory vortical flow, as seen in images (b)–(d) (Refs. 18 and 19).

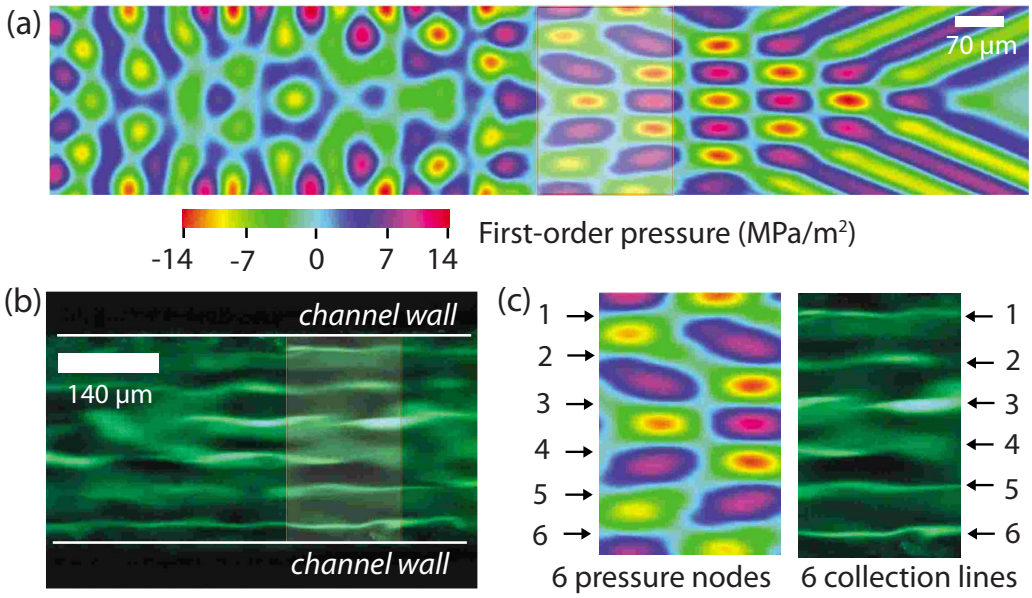

FIG. 12. Comparison between (a) the computed first order pressure field in the fluid and (b) the number of linear 500 nm colloidal particle assemblies that arise in the quiescent fluid region at the bottom of the 280 μm wide microchannel. It can be seen in (c) that the particles appear to collect along the nodes of the pressure field (Refs. 18 and 19).

collection lines is the integer number of nodal lines with separation $\lambda_f/2$ that fit within the given channel width. This then offers specific tunability of the number of particle assemblies, either through the selection of the channel dimension, the fluid or the SAW excitation frequency, which has important implications for particle sorting in microfluidic channels. A particular scheme for microchannel particle focusing using this principle is offered by Shi *et al.*[22]

D. Microcentrifugation

An area that has received little attention so far within microfluidics has been microcentrifugation. Understandably, this is due to the difficulty in generating sufficient centrifugal forces at small scales to overcome the fluid resistance as a consequence of the dominance of surface forces that overwhelm body forces due to the inverse length scaling of the surface area to volume ratio. Strategies to drive effective recirculatory or centrifugal flows in microdevices are therefore required. In an initial conception, small-scale centrifugation was driven through Coriolis forces by rotating an entire disk, similar in size to a compact disk (CD), on which fluidic channels and components were fabricated.[23] This has recently been exploited for separating plasma from whole blood.[24] While quite effective for its desired purpose, such bulk rotation of the entire CD structure, which in itself is relatively large, can, however, be cumbersome, expensive and unreliable—quite the antithesis of microfluidic philosophy. Moreover, the rotation of the entire structure is also nonspecific (i.e., all components on the CD are rotated). This is a severe limitation as there are components upstream or downstream of the reactor or separator, for example, the dispensation and detection components, in which rotation may produce undesirable effects. While it may be possible to isolate merely the reactor and separator to the rotated disk, integration of the rotated structure with the other stationary structures together with fluid connections can be extremely difficult, which is, again, quite contrary to microfluidic philosophy in which integration of all fluid processing components onto a single chip-based device is an end goal.

This first concept of a microcentrifuge, without requiring the bulk rotation of the entire fluidic chamber or any other mechanically moving parts, employed ionic wind, generated through the application of a large electric field to a sharp electrode tip held above a circular microfluidic chamber, to drive bulk air flow which then resulted in fluid recirculation on the surface, and

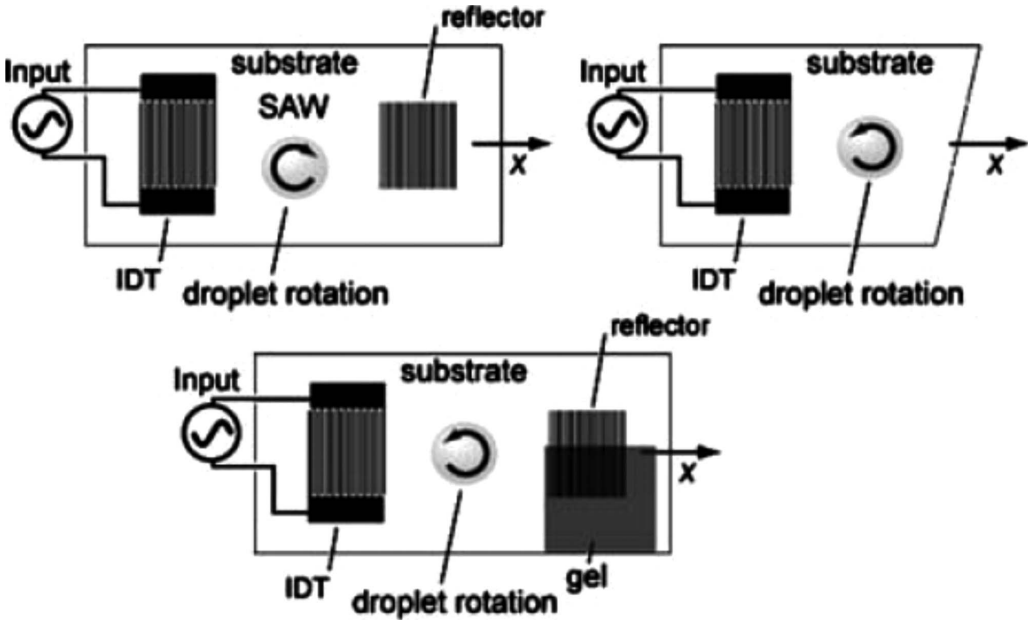

FIG. 13. Azimuthal acoustic streaming within a drop placed on the substrate can be generated by symmetry breaking of the SAW propagation across the substrate either by placing the drop off-center (top-left image) or through asymmetric reflection of the SAW by introducing a diagonal cut at the edge of the substrate (top-right image) or by using absorption (α)-gel to suppress the reflection at one-half of the IDT (bottom image) (Ref. 28).

consequently, beneath the surface in the bulk of the liquid within the chamber through interfacial shear.[25–27] This mechanism was demonstrated as an effective micromixer as well as a mechanism to separate or concentrate particles,[25] for example, the separation of red blood cells from blood plasma.[26,27]

The use of high voltage electric fields and air flows are, however, impractical for a large number of microfluidic systems. A similar microcentrifugatory flow can be generated using SAWs through symmetry breaking of the acoustic wave propagation across the substrate. This can be achieved through various means, as shown in Fig. 13, thus giving rise to azimuthal acoustic streaming within the fluid drop on the substrate.[28] To intensify the azimuthal recirculation, it is possible to employ electric-width-controlled single-phase unidirectional transducer (SPUDT) electrodes in place of the conventional IDT design.[29,30] Unlike the conventional IDT designs, which are bidirectional, i.e., SAWs are produced both to the front and rear of the IDTs, internally tuned reflectors within the IDT fingers in the SPUDT electrode design generates a unidirectional SAW that propagates from only one side of the IDT. Furthermore, the SAW intensity can be increased by focusing the SPUDT using curved electrodes, as shown in Fig. 14(a).[29,30] The corresponding SAW pattern, visualized through laser Doppler vibrometry or simply through smoke particle patterns generated by the SAW on the substrate can be seen in Figs. 14(b) and 14(c), respectively.

Whichever IDT is used, the strong azimuthal streaming within the drop at typical linear velocities of around 1 mm/s with the conventional IDTs and as high as 20 mm/s with the focusing SPUDTs[30] can be exploited to drive intense micromixing or rapid particle separation/concentration. Shilton *et al.*[30] has shown that the chaoticlike inertial flow induced by the SAW provides a means for driving effective turbulent-like mixing, with an enhancement ratio D_{eff}/D_0 that scales roughly as P^2, where D_{eff} is the effective diffusivity, D_0 is the diffusivity in the absence of flow, and P is the power. In Ref. 30, a small amount of food dye is shown to be completely mixed in a glycerine-water drop in under 1 s.

If the drop is suspended with micro/nanoparticles instead, particle concentration or separation can be effected in a related manner, as shown in Fig. 15, in which the particles are continuously drawn into closed azimuthal streamlines and recirculate within the streamline until a critical closed

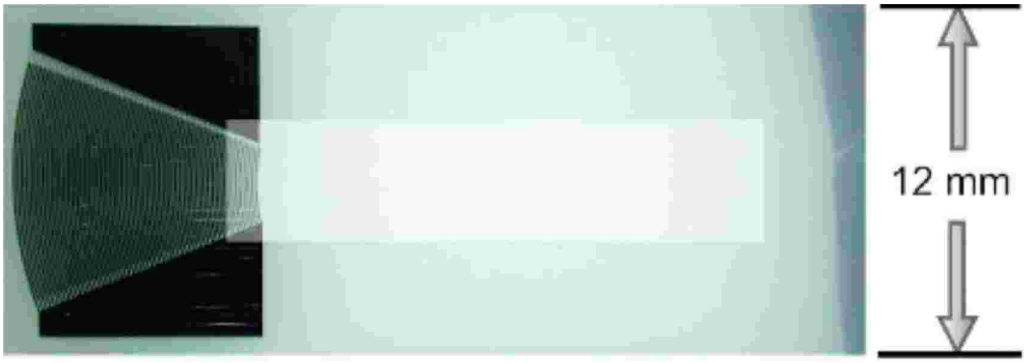

(a)

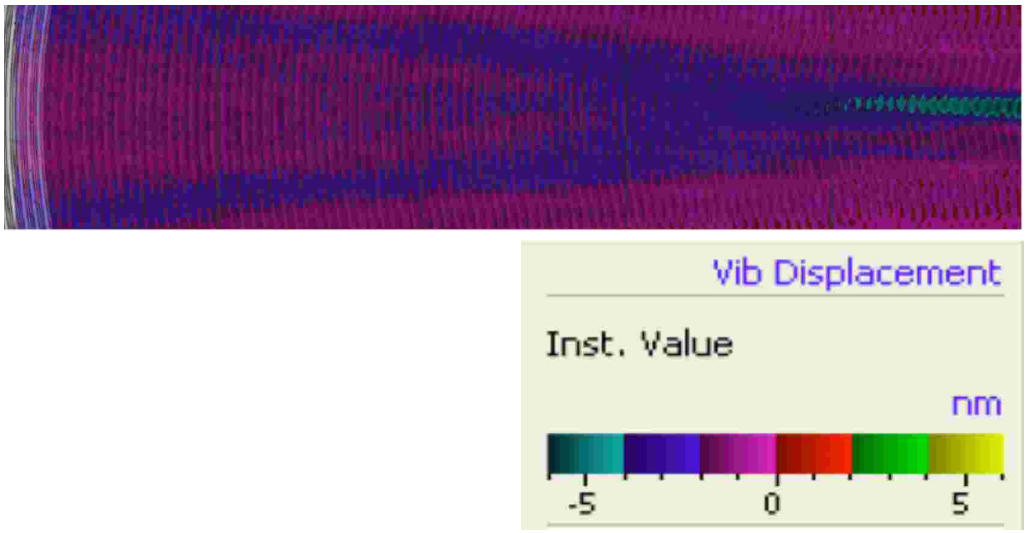

(b)

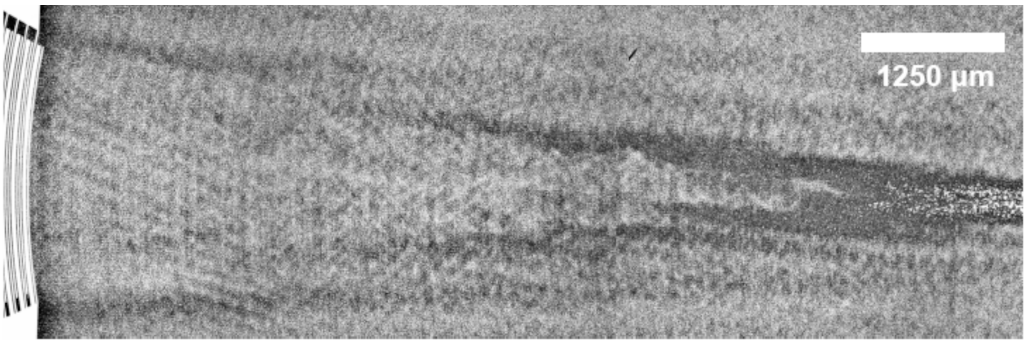

(c)

FIG. 14. (a) Focusing elliptical SPUDT electrode. The corresponding SAW patterns that emerge from the SPUDT, obtained using (b) laser Doppler vibrometry and (c) smoke particle deposition indicate the intensification of the SAW energy towards a focal point (Refs. 29 and 30).

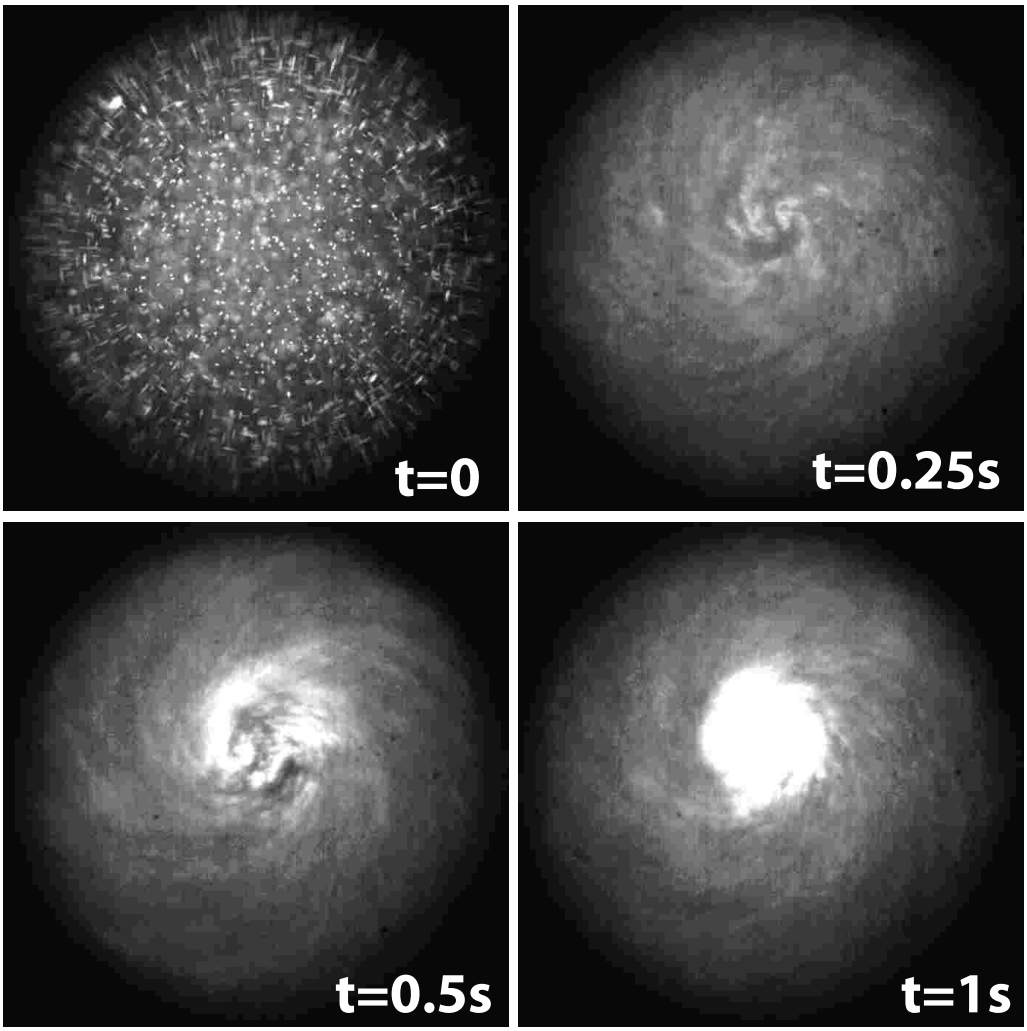

FIG. 15. Rapid concentration of 500 nm fluorescent particles in a 0.5 μL water drop due to the strong inertial bulk fluid recirculation induced by the SAWs generated using elliptical focusing SPUDTs (Ref. 30).

packing fraction is reached beyond which shear gradients induce cross-streamline transport causing the particles to migrate towards the center of the vortex structure. Unlike the ionic wind driven microcentrifugation, which requires several minutes, for example for the blood cells to concentrate and hence the plasma layer to be separated, the SAW-driven inertial microcentrifugatory flow occurs in under 1 s. Besides blood plasma separation as a requisite precursor stage for blood diagnostics on a microfluidic platform, the mechanism also constitutes a rapid preconcentration step, for example, to facilitate easier and faster pathogen detection in microfluidic biosensors. Another salient attribute of the azimuthal flow permits further microfluidic manipulation. Li *et al.*[28] report an optimum rf power input for concentration, beyond which, the increasingly intense acoustic streaming drives strong inertial convection which then overwhelms shear diffusion such that the particles redisperse. This therefore offers the capability of controlled particle concentration and dispersion at will.

E. Jetting

A recently discovered SAW jetting phenomenon offers further exciting possibilities for a wider range of microfluidic applications. This was demonstrated by Tan *et al.*[31] who used two

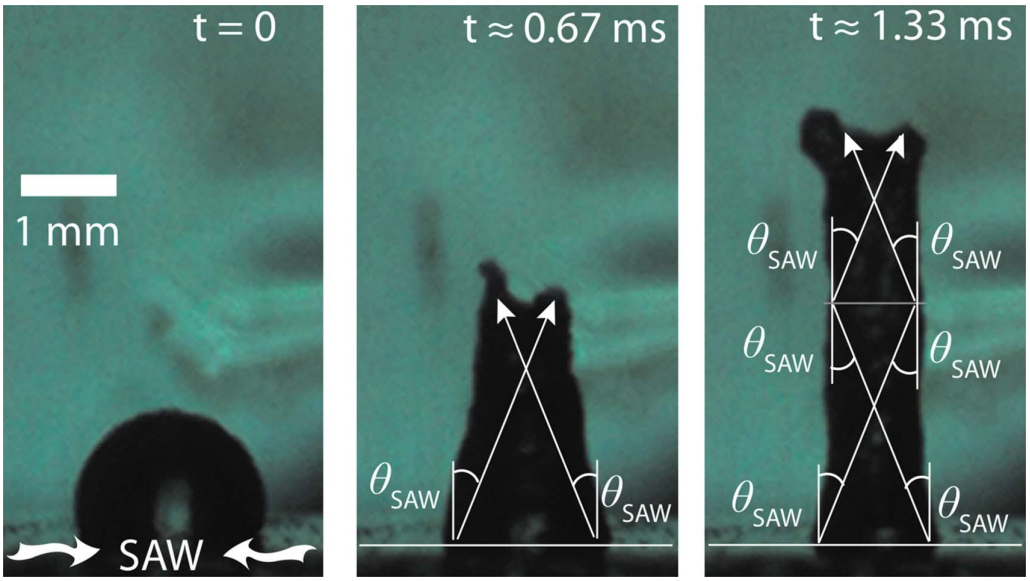

FIG. 16. Initial stages of the jet formation as a consequence of the concentration of acoustic radiation into the drop arising as a consequence of the convergence of two SAWs produced by elliptical focusing SPUDTs placed on both sides of the drop (Ref. 31).

elliptical focusing SPUDTs at two opposite ends of the substrate to drive the convergence of two SAWs at a point above which a liquid drop is placed. The transmission of radiation at the Rayleigh angle into the liquid from both the front and rear sides of the drop causes it to deform into a coherent elongated liquid column, as observed in Fig. 16. Such jetting phenomena, without requiring fluid confinement mechanisms such as nozzles or orifices to accelerate the fluid to adequately sufficient velocities requisite to produce elongated jets, demonstrates the ability for the SAW to drive strong inertial forcing on a liquid that is unique in microfluid flows. In any case, the jets observed here present opportunities for ink-jet or soft biological printing and fiber synthesis, among other applications; in the latter, the inability of the SAW to denature biomolecules represent an advantage over other techniques that involve high shear or large electrical currents.

The rich dynamics of the SAW jetting phenomenon is captured in Fig. 17, in which we observe the jet length and the ability to initiate single droplet or even multiple droplet ejection, the former due to tip pinch-off and the latter as a consequence of the axisymmetric breakup of the cylindrical jet column associated with the classical Rayleigh–Plateau instability, to depend on the jet Weber number, defined as $\mathrm{We}_j \equiv \rho U_j^2 R_j / \gamma$, where ρ is the fluid density, U_j is the jet velocity, R_j is the jet radius, and γ is the interfacial tension.

F. Atomization

At high powers, the displacement velocity of the substrate as the SAW passes along its surface is typically 1 m/s irrespective of the excitation frequency. Given the 10 nm order amplitude of the SAW, the surface acceleration is therefore extremely large, on the order of 10^7–10^8 m^2/s. These huge accelerations, in turn, induce strong capillary waves at the free surface of the drop, which, when sufficiently strong to overcome the capillary stress, destabilizes the interface and leads to atomization of the drop. The atomized droplets are highly monodisperse and around 1–10 μm in size, roughly insensitive to the SAW frequency due to the viscous damping of the drop, in which case the capillary waves at the free surface of the drop vibrate at a frequency associated with viscous-capillary resonance.[32] If the drop, prior to atomization, were to, however, spread into a film that is thinner than the thickness of the compressional boundary layer adjacent to the substrate, approximately 0.1–1 μm for water, where inertial effects are dominant due to the extremely large surface acceleration off the substrate, the free surface of the film undulates at a

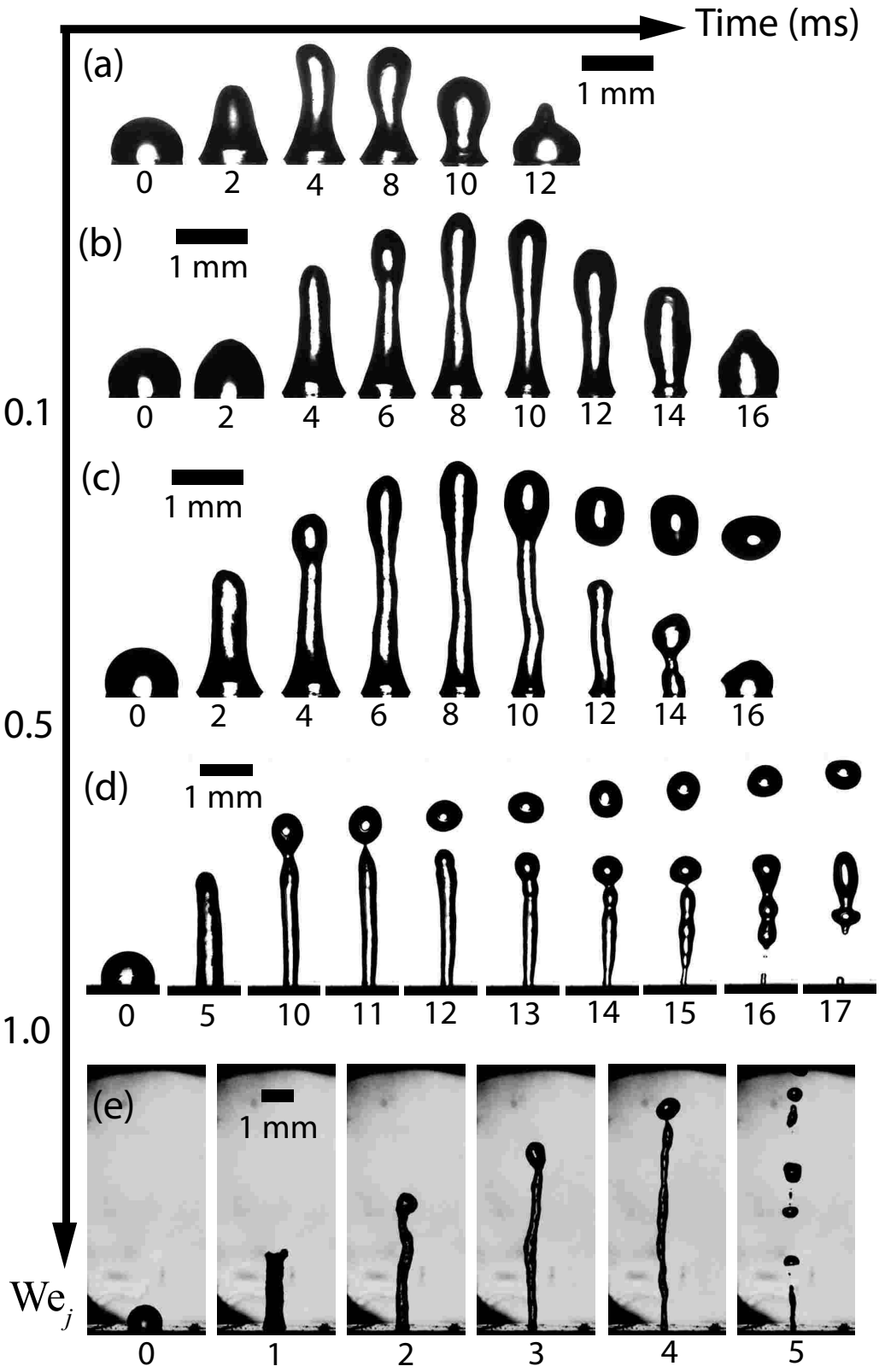

FIG. 17. Time sequence of the SAW jets produced, showing the dependence of its length and breakup as a function of the Weber number We_j (Ref. 31).

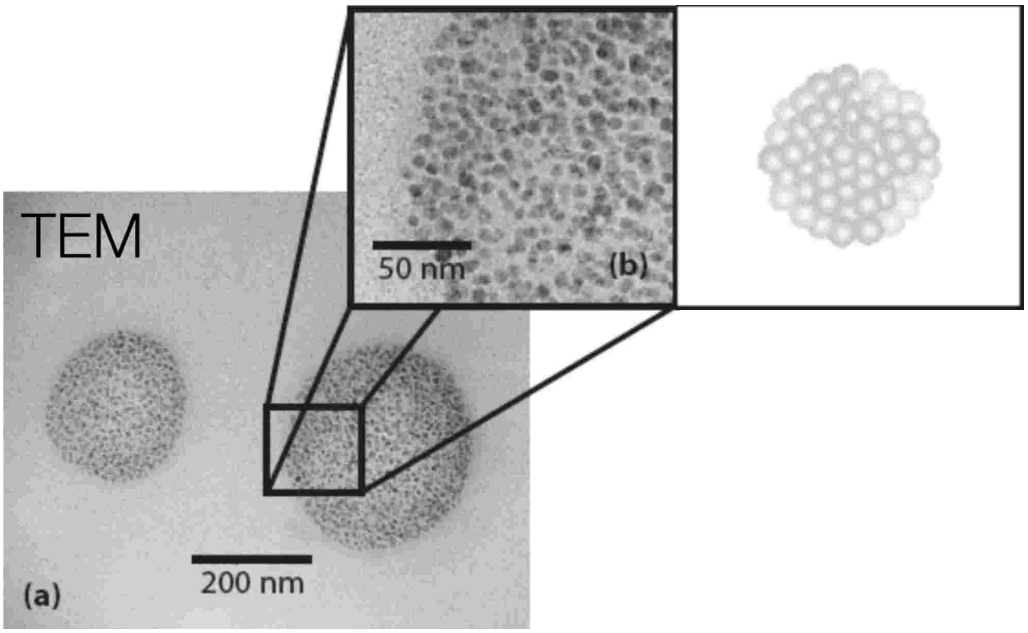

FIG. 18. 150–200 nm polymer nanoparticles synthesized using the SAW atomization technique. (a) Transmission electron microscopy image of a nanoparticle. (b) Magnification of the image showing the sub-50 nm particulates that aggregate to form the 200 nm cluster; the schematic shows a three-dimensional reconstruction of the particle aggregate that resembles a grape bunch (Ref. 33).

frequency associated with inertial capillary resonance, in which case the atomized droplets may be below 1 μm.[32] This inertial film destabilization can be exploited for producing regular spatially homogeneous polymer spot patterns, as will be discussed subsequently.

Whichever the case, SAW atomization presents a rapid and simple technique for the generation of micron and submicron aerosol droplets for a wide range of industrial processes such as ink-jet printing, agricultural spraying, fuel injection, pulmonary drug delivery, and DNA microarray printing. We note that the monodispersed micron order droplets are particularly well-suited for pulmonary drug delivery in which 2–5 μm order aerosol drops are typically prescribed for optimum dose efficiency in order to deliver the maximum amount of drug to the lower respiratory airways for direct local administration to target organs. The power required for atomization, around 1 W, is at least one order of magnitude smaller than that of ultrasonic atomizers that employ Langevin transducers and single lead zirconium titanate element thickness-mode piston atomizers, which operate in the 10 kHz–1 MHz frequency range. Another advantage of the SAW atomization technique, as with the jetting phenomena discussed above, is the ability to do away with nozzles and orifices, thus simplifying considerably the device, and hence, reducing its costs and increasing its reliability.

The technique can also be used as a straightforward method for generating biodegradable polymeric nanoparticles simply by atomizing a solvent drop in which the polymeric excipient is dissolved.[33] The subsequent in-flight evaporation of the atomized solvent droplets then leaves behind solidified polymeric particles which are relatively monodispersed. Due to the rapid temperature quenching that arises as a consequence of the high drop ejection velocities, the nonuniform surface evaporation that occurs results in spatial inhomogeneities in the polymer/solvent concentration and ultimately the production of 150–200 nm spherical clusters comprising sub-50 nm particulates. These clusters resemble grape bunches, as illustrated in the schematic in Fig. 18.[33] In any case, the one-step process for synthesizing these nanoparticles constitutes an attractive alternative to the slow and cumbersome multistep conventional methods, e.g., spray drying, nanoprecipitation, emulsion photocross-linking, etc.

Alvarez *et al.* also demonstrated the SAW atomization process to be useful for generating

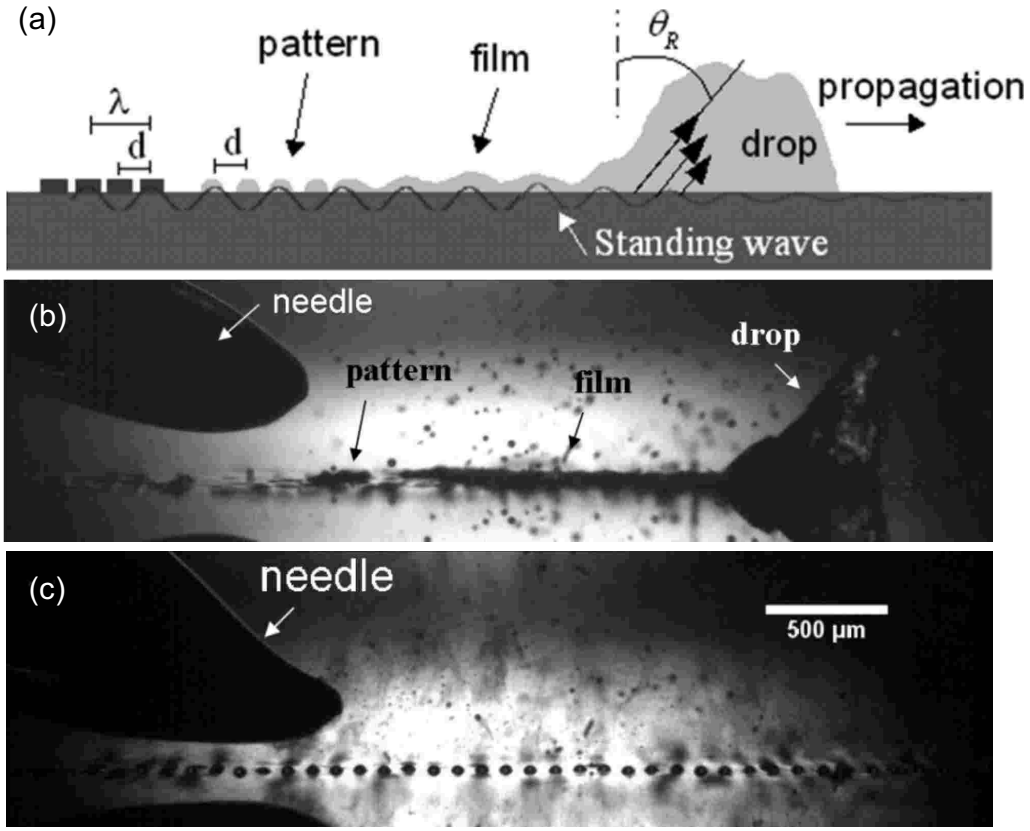

FIG. 19. Self-organization of regular polymer spot patterns. A drop of polymer solution dispensed from the needle above the SAW substrate [(a), (b)] translates under the SAW leaving behind a thin trailing film, which subsequently destabilizes leading towards atomization and evaporation of the solvent, thus leaving behind (c) solified polymer spot patterns (Ref. 36).

100 nm order protein (insulin) nanoparticles as well as 3 μm aerosol droplets for inhalation therapy.[34] Furthermore, it is possible to load the protein and other therapeutic molecules into the biodegradable polymer nanoparticle shells as a vehicle for controlled release drug delivery.[35] The encapsulation of the drug within the biodegradable polymer essentially shields the drug from rapid hydrolysis and degradation, allowing sustained release over time, thus prolonging the effect of the drug over longer periods whilst preventing dangerous dose spikes. Encapsulation is typically a delicate procedure that can damage the protein during the process through denaturization or aggregation; nevertheless, preliminary tests have indicated the viability of the protein after SAW atomization, especially at the high frequencies employed, in the same way that SAW irradiation does not affect the viability and proliferation of stem cells, as discussed previously in Sec. II B.

In addition, the SAW atomization offers the potential for the controlled production of regular, long-range, spatially ordered polymer spot patterns without requiring physical/chemical substrate templating or other surface treatment procedures.[36] The self-organization of these polymer patterns involves a two-step procedure. As shown in Figs. 19(a) and 19(b), the translation of a drop containing the polymer solution leaves behind a thin trailing film, which simultaneously destabilizes. Consequently, the violent free surface vibrations causes thinning at the antinodes of the standing SAW vibration on and transverse to the substrate, resulting in the depletion of the film at these positions. This is compounded by the evaporation of the solvent, the rate of which is locally enhanced where there is significant film thinning. The breakup of the film across the entire substrate surface at the antinodal positions, both axially and transversely, and the subsequent solvent evaporation, then produces evenly spaced solidified polymer droplets, as shown in Figs.

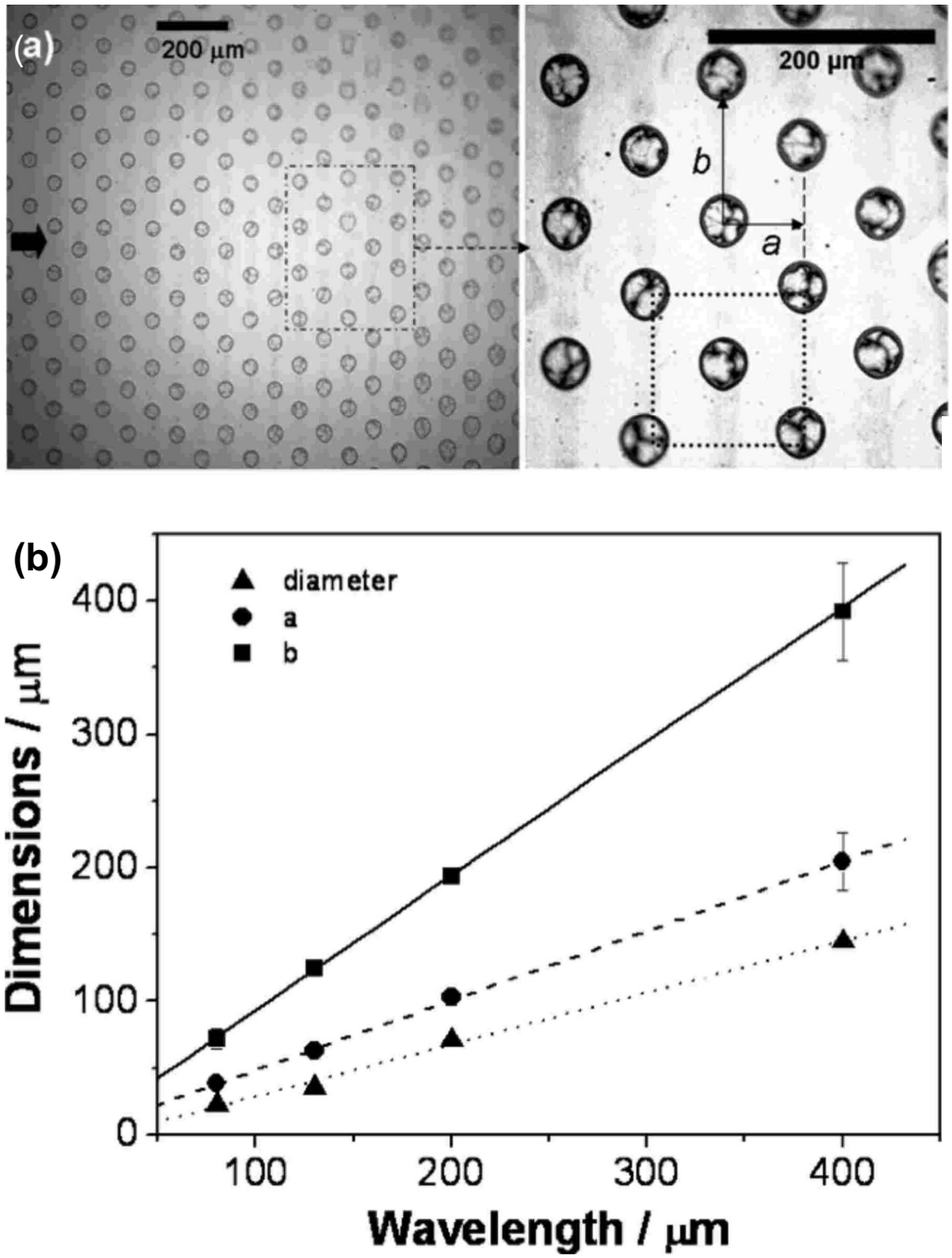

FIG. 20. (a) The two-dimensional array of polymer spots produced by the SAW translation and atomization process is extremely regular and organized. (b) The spot diameter, longitudinal pitch spacing a and transverse pitch spacing b [see image (a)] are strongly correlated to the SAW frequency, and hence, wavelength (Ref. 36).

19(c) and 20(a). We note the dependence of the pattern periodicity as well as the polymer spot size on a lone parameter, namely the SAW frequency (or wavelength), as observed in Fig. 20(b), therefore endowing the process with the ability for controllability and fine tuning, which is a key advantage over other conventional patterning methods.[36]

III. PERSPECTIVES AND FUTURE DIRECTIONS

The wide and varied range of fluid actuation and particle manipulation capabilities discussed above reveal the enormous potential for the use of SAWs in micro/nanofluidics. Although there are many advantages with the use of SAWs, including its low cost, ease of fabrication, scaleability, simplicity, and efficiency, its biggest assets are its ability to drive extremely fast motion, one to two orders of magnitude faster than that currently capable with other microfluidic actuation mechanisms, and strong inertial motion, which is not possible in most microfluidic devices. Given the infancy of SAW microfluidics, we expect significant growth in interest as well as research in this area in the coming decade in a similar way to which electrokinetics has progressed to date. We note, in particular, that SAW sensors, and to a lesser extent, SAW biosensors, are already at a mature development stage (see, for example, Ballantine *et al.*[37] and Länge *et al.*[38]), which is a reason why we have deliberately refrained from a discussion on these in this article. Such technology therefore offers tremendous opportunities for the integration of SAW microfluidic and SAW sensor platforms for miniature chemical and biological sensing. We expect that this will constitute a significant body of research effort in the near future once the SAW microfluidic technology progressively matures.

In the meantime, however, much is left to be done, both in terms of acquiring a deeper fundamental understanding of the mechanisms that govern the SAW-driven fluid and particle interaction, as well as developing a robust integrated microfluidic platform for specific lab-on-a-chip applications. In the former, new fluid phenomena continue to be discovered, which require further rigorous investigation to elucidate the complex, nonlinear fluid-structural interactions and physicochemical hydrodynamics underlying the processes observed. For example, there is yet to be an extensive understanding of the complicated three-dimensional flow behavior associated with acoustic streaming in a sessile drop, let alone the added complexity of acoustic radiation and hydrodynamic effects on particles suspended within the drop. How drops translate under the SAW forcing, and in particular, the dynamics in the advancing and receding contact line region, are also not well understood. Moreover, a thorough comprehension of the free surface behavior of the drop or a film excited by the SAW underneath it remains elusive—although progress has been made to understand the mechanisms governing the vibrations occurring at the free surface (see, for example, Qi *et al.*[32]), a detailed theoretical model that captures the capillary wave excitation and destabilization leading towards droplet pinch-off and jetting is urgently needed. Significant challenges arise, however, posed by the large length and time scale separation between the SAW wavelength (and frequency) with the characteristic length and period associated with the hydrodynamics, thus rendering the numerics associated with the problem extremely stiff.

On the development aspect, the requirement of the piezoelectric substrate presents a significant limitation to the material in which the device can be fabricated from. Fortunately, recent results have hinted at the possibility, with the aid of a fluid layer atop the piezoelectric substrate, of coupling the SAW radiation through a superstrate, while retaining the possibility for driving similar fluidic actuation and particle manipulation, albeit in a drop placed on the superstrate.[39] The superstrate itself could consist of typical materials from which microfluidic chips are fabricated, for example, silicon or PDMS, thus decoupling the SAW driving circuit from the microfluidic device. This is an exciting possibility since the more expensive SAW device could be reused whereas the cheaper microfluidic circuits which eventually become contaminated with, for example, biological samples, can be disposed of after use. The acoustic radiation as it evolves through the fluid coupling layer, the superstrate, and the fluid atop the superstrate, however, needs to be further characterized.

ACKNOWLEDGMENTS

We are especially indebted to our team of extremely dedicated students and postdoctoral associates at the Micro/Nanophysics Research Laboratory with whom we have enjoyed sharing the journey in unraveling the many intricacies and peculiarities of surface acoustic wave microfluidics. In alphabetical order, these are M. Alvarez, D. R. Arifin, M. Bok, R. P. Hodgson, S. Kan-

dasamy, K. Kulkarni, H. Li, A. Qi, R. Raghavan, P. Rogers, R. Shilton, and M. K. Tan. Our collaborators, M. I. Aguilar (Biochemistry and Molecular Biology, Monash University), H.-C. Chang (Chemical and Biomolecular Engineering, University of Notre Dame), A. Dasvarma (Australian Stem Cell Centre), K.-Y. Hashimoto (Electrical and Electronics Engineering, Chiba University), T.-H. Lee (Biochemistry and Molecular Biology, Monash University), A. Mechler (Chemistry, Monash University), O. K. Matar (Chemical Engineering and Chemical Technology, Imperial College London), P. Perlmutter (Chemistry, Monash University), P. Stoddart (Centre for Atom Optics and Spectroscopy, Swinburne University), and K. Traianedes (Australian Stem Cell Centre) also deserve mention for their helpful advice and insightful discussions on the topic. In addition, we are grateful for the funding bodies that have enabled various aspects of this work, including the Australian Research Council (Discovery Project Nos. DP0666549, DP0666660, and DP0773221; Linkage, Infrastructure, Equipment and Facilities LP0668435), Nanotechnology Victoria, and the Research Support for Counter-Terrorism program administered by the Department of Prime Minister and Cabinet's Office of National Security.

[1] H. A. Stone, A. D. Stroock, and A. Ajdari, Annu. Rev. Fluid Mech. **36**, 381 (2004).
[2] T. M. Squires and S. R. Quake, Rev. Mod. Phys. **77**, 977 (2005).
[3] S. Bao, B. D. Thrall, and D. L. Miller, Ultrasound Med. Biol. **23**, 953 (1997).
[4] Lord Rayleigh, Proc. London Math. Soc. **s1–17**, 4 (1885).
[5] R. White and F. Voltmer, Appl. Phys. Lett. **7**, 314 (1965).
[6] C. K. Campbell, *Surface Acoustic Wave Devices for Mobile and Wireless Communications* (Academic, Orlando, FL, 1998).
[7] H. Li, J. R. Friend, and L. Y. Yeo, Phys. Rev. Lett. **101**, 084502 (2008).
[8] G. Falkovich, A. Weinberg, P. Denissenko, and S. Lukaschuk, Nature (London) **435**, 1045 (2005).
[9] A. Renaudin, P. Tabourier, V. Zhang, J. C. Camart, and C. Druon, Sens. Actuators B **133**, 389 (2006).
[10] M. K. Tan, J. R. Friend, and L. Y. Yeo, Lab Chip **7**, 618 (2007).
[11] L. Y. Yeo and H.-C. Chang, Mod. Phys. Lett. **19**, 549 (2005).
[12] J. Zeng and T. Korsmeyer, Lab Chip **4**, 265 (2004).
[13] J.-Y. Yoon and R. L. Garrell, Anal. Chem. **75**, 5097 (2003).
[14] Z. Guttenberg, H. Müller, H. Habermüller, A. Geisbauer, J. Pipper, J. Falbel, M. Kielpinski, J. Scriba, and A. Wixforth, Lab Chip **5**, 308 (2005).
[15] H. Li, J. R. Friend, and L. Y. Yeo, Biomaterials **28**, 4098 (2007).
[16] M. Bok, H. Li, L. Y. Yeo, and J. R. Friend, Biotechnol. Bioeng. (in press).
[17] H. Li, L. Y. Yeo, J. R. Friend, A. Dasvarma, and K. Traianedes, preprint.
[18] M. K. Tan, J. R. Friend, and L. Y. Yeo, Proceedings of the 16th Australasian Fluid Mechanics Conference, Gold Coast, Queensland, Australia, 2007, University of Queensland, Brisbane, 2007 (unpublished).
[19] M. K. Tan, L. Y. Yeo, and J. R. Friend, Phys. Rev. Lett. (submitted).
[20] S. Girardo, M. Cecchini, F. Beltram, R. Cingolani, and D. Pisignano, Lab Chip **8**, 1557 (2008).
[21] D. J. Laser and J. G. Santiago, J. Micromech. Microeng. **14**, R35 (2004).
[22] J. Shi, X. Mao, D. Ahmed, A. Colletti, and T. J. Huang, Lab Chip **8**, 221 (2008).
[23] M. J. Madou and G. J. Kellogg, in *Systems and Technologies for Clinical Diagnostics and Drug Discovery*, edited by G. E. Cohn and A. Katzir (SPIE, San Jose, CA, 1998) Vol. 3259, pp. 80–93.
[24] S. Haeberle, S. Brenner, R. Zengerle, and J. Ducree, Lab Chip **6**, 776 (2006).
[25] L. Y. Yeo, D. Hou, S. Maheshswari, and H.-C. Chang, Appl. Phys. Lett. **88**, 233512 (2006).
[26] L. Y. Yeo, J. R. Friend, and D. R. Arifin, Appl. Phys. Lett. **89**, 103516 (2006).
[27] D. R. Arifin, L. Y. Yeo, and J. R. Friend, Biomicrofluidics **1**, 014103 (2007).
[28] H. Li, J. R. Friend, and L. Y. Yeo, Biomed. Microdevices **9**, 647 (2007).
[29] M. K. Tan, J. R. Friend, and L. Y. Yeo, Appl. Phys. Lett. **91**, 224101 (2007).
[30] R. Shilton, M. K. Tan, L. Y. Yeo, and J. R. Friend, J. Appl. Phys. **104**, 014910 (2008).
[31] M. K. Tan, J. R. Friend, and L. Y. Yeo, Phys. Rev. Lett. (submitted).
[32] A. Qi, L. Y. Yeo, and J. R. Friend, Phys. Fluids **20**, 074103 (2008).
[33] J. R. Friend, L. Y. Yeo, D. R. Arifin, and A. Mechler, Nanotechnology **19**, 145301 (2008).
[34] M. Alvarez, J. R. Friend, and L. Y. Yeo, Nanotechnology **19**, 455103 (2008).
[35] M. Alvarez, L. Y. Yeo, and J. R. Friend, Biomicrofluidics (in press).
[36] M. Alvarez, J. R. Friend, and L. Y. Yeo, Langmuir **24**, 10629 (2008).
[37] D. S. Ballantine, R. M. White, S. J. Martin, A. J. Ricco, E. T. Zellers, G. C. Frye, and H. Wohltjen, *Acoustic Wave Sensors: Theory, Design & Physico-Chemical Applications* (Academic, San Diego, 1997).
[38] K. Länge, B. E. Rapp, and M. Rapp, Anal. Bioanal. Chem. **391**, 1509 (2008).
[39] J. R. Friend, L. Y. Yeo, M. K. Tan, and R. P. Hodgson, Appl. Phys. Lett. (in press).